Effect of Chemical Composition on Large Deformation Mechanooptical Properties of High Strength Thermoplastic Poly(urethane urea)s

Sezen Curgul

Department of Mechanical Engineering, Koc University, Rumelifeneri Yolu 34450 Istanbul, Turkey

Iskender Yilgor and Emel Yilgor

Department of Chemistry, Koc University, Rumelifeneri Yolu 34450 Istanbul, Turkey

Burak Erman*

Department of Chemical and Biological Engineering, Koc University, Rumelifeneri Yolu 34450 Istanbul, Turkey

Miko Cakmak

Institute of Polymer Engineering, University of Akron, Akron, Ohio 44325-0301

Received May 18, 2004; Revised Manuscript Received July 12, 2004

ABSTRACT: The effect of composition on the true mechanooptical properties of thermoplastic poly(urethane urea)s was investigated by selectively varying the type and content of soft and hard segments. Real-time stress−strain−birefringence data together with off-line wide-angle X-ray scattering measurements revealed that soft segment and chain extender play dominant roles on the chemical structures of the poly(urethane urea)s. All poly(tetramethylene oxide) glycol-based samples showed the same crystal structure. The samples containing ethylenediamine as the chain extender showed enhanced crystallizability as compared to those with 1,6-diaminohexane no matter which soft segment was used. In general, samples with lower fraction of hard segment exhibited higher crystallizability than their high hard segment counterparts. Long-term holding of poly(ethylene oxide) samples in stretched state was found to increase crystallinity. The strain-induced crystallization in low hard segment content poly(tetramethylene oxide)-based samples was only observed at very high deformation levels. On the other hand, crystallization in the samples containing high hard segment was found to evolve gradually over large deformation range. The strain rate has a considerable effect on the crystallization behavior of poly(tetramethylene oxide)-based samples. While the low hard segment content poly(tetramethylene oxide) sample experiences decreasing crystallizability as the strain rate increases, its counterpart containing higher fraction of hard segments exhibits opposite behavior. We have investigated linear and nonlinear stress optical behavior and observed that the span of the initial linear stress optical region varied primarily with composition (slope ranging from 0.1 to 2.2 GPa^{-1}) and secondarily with the deformation rate. Hysteresis experiments show that there is a considerable loss of energy in cyclic loading of these materials, and hysteresis increases as the chain extender is changed from 1,6-diaminohexane to ethylenediamine.

Introduction

Segmented poly(urethane urea)s are linear macromolecules made of alternating sequences of soft and hard segments. The soft segments usually consist of the polyether or poly(ester glycol)s, whereas the hard segments consist of diisocyanate and a diol or diamine chain extender. Depending on the concentration and type of these units, thermoplastic poly(urethane urea)s (TPUUs) can have various desirable properties including high strength, good abrasion resistance, high elongation to break, and high modulus of elasticity when compared to many other elastomers. The main mechanism underlying these unique properties is the phase separation of the hard and soft segments that have been the subject of several previous studies.

Cooper and Tobolsky[1] were the first to propose a phase-separated domain morphology for elastomeric polyurethanes in 1966. From that time on, the unique properties of polyurethanes have been associated with microphase separation of the hard and soft segments, in which the continuous soft segment matrix provides the elastomeric behavior while hard segments provide physical cross-linking and high strength. Thermodynamic driving forces and the kinetic paths are the two main factors that determine the amount and type of microphase separation. The difference between the solubility parameters of hard and soft segments also has a strong influence on the degree of microphase separation.

The microstructure of these materials was first investigated using X-ray diffraction by Clough et al.[2,3] Bonart[4] proposed that upon deformation hard segments orient in transverse direction up to a certain stretch ratio and then orient in the stretching direction. He also suggested that stress-induced crystallization begins in soft segments as a result of decrease in entropy. Many other models have been suggested to describe the domain structure of phase-separated polyurethanes based upon X-ray and other indirect viscoelastic measurements and thermal analysis.[5−7] Estes et al.[6] proposed a morphology in which both phases are represented as being continuous and interpenetrating, yet not completely phase separated. Bonart[7] explained a three-dimensional model taking interurethane hydrogen bond-

* Corresponding authors. E-mail berman@ku.edu.tr.

10.1021/ma049018a CCC: $27.50
Published on Web 10/19/2004

ing into account. Wilkes[8] suggested that hard segments orient either radially or tangentially in the spherulites in order to explain the different types of optical symmetry observed.

Sung et al.[9] studied the mechanical properties of polyurethanes in order to demonstrate the consequences of phase segregation and domain structures. Increasing the molecular weight of the PTMO soft segment was found to enhance phase segregation and improve mechanical properties, resulting in higher elongation at break, greater toughness, lower hysteresis, and a slower rate of stress relaxation. In addition to the soft segment, hard segment also plays a major role in microphase separation. Cooper et al.[10] observed a transition of morphology from interconnecting hard and soft segment domains to isolated hard segment domains in a soft segment matrix upon decreasing the hard segment content (HS). They concluded that small differences in the orientation behavior of the hydrogen-bonded and nonbonded urethane units at the hard domain interface could lead to the slightly different morphology of each sample. Increasing the segmental length of hard segments can increase the amount of phase separation.[11,12] Increasing the hard segment content results in larger hard segment domain sizes and higher hard segment domain concentrations in the soft segment matrix.[13]

Most TPUUs are highly elastomeric and can be elongated to very high stretch ratios. Releasing the applied strain results in quick and complete recovery of the original shape. This extraordinary behavior makes these materials suitable for many applications involving cyclic loading. Infrared orientational studies of hysteresis[14] showed that plastic deformation occurs predominantly in hydrogen-bonded hard segment domains. The hysteresis is due to the disruption of the structure in the hard segment aggregates. Also, the soft and hard segments residing in the soft phase show substantial recovery upon unloading. According to SAXS data of Desper et al.,[15] the hard segment phase breaks up into smaller chunks, compromising their physical cross-linking effect, leading to higher mechanical hysteresis. The second elongation was found to produce a higher stress than the stress reached in the previous cycle.[16] It was then concluded that the ordered hard segment regions break upon elongation and reconstruct partially upon recovery. Some studies[17,18] differentiated between hysteresis at small and large strains, indicating that low mechanical hysteresis that occur at small strains does not permanently disrupt the morphology of the polymer. An increase in mechanical hysteresis at higher strains is attributed to morphological changes and to processes that lead to permanent deformation.

As discussed above, TPUUs show a complex morphological behavior that strongly depends on their chemical compositions and backbone structures. In this study, a new series of TPUUs were synthesized, and information regarding their mechanooptical properties was acquired using a uniaxial stretching apparatus in combination with offline wide-angle X-ray (WAXS) studies. What makes this study different from other studies is that the polyurethanes under consideration are unique, and they are high-strength TPUUs which can function under heavy loading conditions (up to 40 MPa). Another fact is that the uniaxial stretching instrument, the details of which are given elsewhere,[19,20] is capable of measuring true stress−strain values online together with birefringence, thus allowing a unique look at the mechanooptical behavior at wide range of deformation levels and strain rates.

Table 1. Polymer Codes and Compositions of the TPUUs

group no.	code	polyol/diisocyanate/chain extender
1	PT-HMDA-20	PTMO/HMDI/HMDA
	PT-HMDA-30	PTMO/HMDI/HMDA
2	PT-ED-20	PTMO/HMDI/ED
	PT-ED-30	PTMO/HMDI/ED
3	PE-HMDA-20[a]	PE/HMDI/HMDA
	PE-HMDA-30	PE/HMDI/HMDA
4	PE-ED-20[a]	PE/HMDI/ED
	PE-ED-30	PE/HMDI/ED

[a] The actual hard segment content is 22.7%.

Experimental Procedure

Materials. Bis(4-isocyanatocyclohexyl)methane (HMDI) with a purity higher than 99.5% was obtained from Bayer AG, Leverkusen, Germany. Poly(tetramethylene oxide) glycol (PTMO) with a number-average molecular weight (M_n) of 2040 g/mol was received from Du Pont. α,ω-Amine-terminated poly(ethylene oxide) oligomer (PEO) (Jeffamine ED2003) (M_n = 1975 g/mol, from end group titration) was kindly provided by Huntsman Corp. Reagent grade ethylenediamine (ED), 1,6-diaminohexane (HMDA), dimethylformamide (DMF), and 2-propanol (IPA) were obtained from Aldrich. Dibutyltin dilaurate (DBTDL) catalyst was obtained from Witco. Water contents of PTMO, PEO, and DMF were determined by Karl Fisher titration and were found to be less than 300 ppm. All chemicals and solvents were used as received.

Polymer Synthesis. A two-step procedure was followed during the preparation of segmented TPUU copolymers. The first step was the formation of an isocyanate-terminated prepolymer, followed by chain extension to form high molecular weight copolymers. PTMO-based prepolymers were prepared in a four-neck, flat bottomed 1 L Pyrex reaction kettle fitted with an overhead stirrer, addition funnel, thermometer, and dry nitrogen inlet. The kettle was charged with calculated amounts of HMDI and PTMO, heated to 80 °C, and stirred. The reaction was started by the addition of 0.005 g of DBTDL catalyst in 1 mL of toluene, followed by FTIR spectroscopy, monitoring the disappearance of sharp isocyanate peak at 2270 cm^{-1} and broad hydroxyl peak at 3400 cm^{-1} and formation of strong urethane (C═O) and (N−H) peaks at 1750 and 3300 cm^{-1}, respectively, using a Nicolet Impact 400D spectrometer. Prepolymer formation was generally completed in 2 h. Isocyanate content of the prepolymer was determined. The prepolymer was dissolved in 250 g of DMF, and the solution was cooled to room temperature before chain extension.

PEO-based prepolymers were also prepared in a four-neck, 1 L Pyrex reaction flask fitted with an overhead stirrer, addition funnel, thermometer, and dry nitrogen inlet. HMDI was weighed into the kettle and dissolved in IPA. A calculated amount of PEO was separately dissolved in IPA and introduced into an addition funnel. Prepolymer was prepared by the dropwise addition of PEO into the reactor at room temperature. Completion of the reaction was confirmed by FTIR spectroscopy. For chain extension calculated amounts of diamine chain extenders (ED, HMDA) were dissolved in IPA, introduced into the addition funnel, and added into the prepolymer solution at room temperature under strong agitation. The reactions were followed by FTIR spectroscopy, monitoring the disappearance of sharp isocyanate peak at 2270 cm^{-1}. Toward the end of the chain extension process as the viscosity of the reaction medium increased, reaction mixture was diluted by the addition of IPA.

Table 1 provides the codes and chemical compositions of poly(urethane urea) and polyurea copolymers prepared and investigated in this study.

As shown in Table 1, eight different samples falling into four groups according to their chemical structures were prepared and characterized. The first column gives the group number. The second column provides the coding, which works

Table 2. Chemical Structures of the Materials

Group No.	Material	Composition
1	PT-HMDA	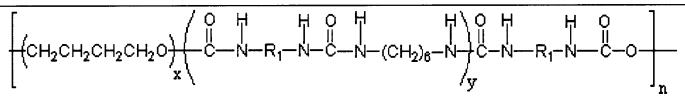
2	PT-ED	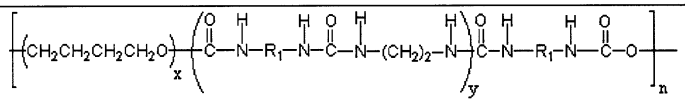
3	PE-HMDA	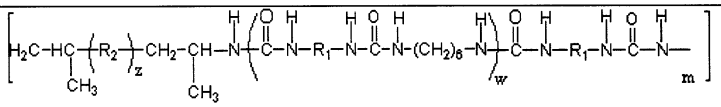
4	PE-ED	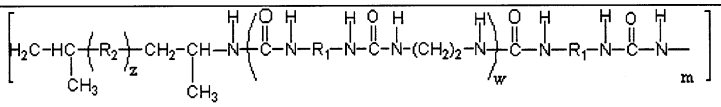

as follows: the first two letters indicate the soft segment type (PT = PTMO and PE = PEO), the next two- or four-letter code denotes the chain extender, and the two-digit number that follows shows the weight percent of the hard segment in the copolymer. In the third column, individual components that constitute the chemical composition of the copolymers are given in the following order: polyol/diisocyanate/chain extender. All copolymers were prepared from the same diisocyanate, HMDI. The chain extender is either HMDA or ED.

The samples listed in Table 1 are divided into four groups, each with different combinations of the soft segments and chain extenders: (i) Samples in the first group have PTMO as their soft segment and HMDA as the chain extender. (ii) Group 2 samples have PTMO as the soft segment and ED as the chain extender. (iii) Samples in group 3 have PEO as the soft segment and HMDA as the chain extender. (iv) Samples in the fourth group have PEO as the soft segment and ED as the chain extender.

In Table 2, R_1 indicates a dicyclohexylmethane radical. R_2 is PEO with the following structure, where b is approximately 39 and $a + c$ is 6.

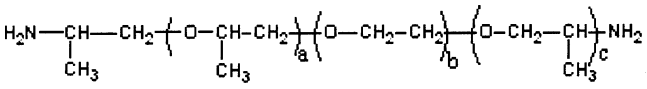

Detailed chemical structures of the four groups of polymers shown in Table 1 are presented in Table 2. The first column denotes the nomenclature adopted in this study. The number of repeat units (x) is around 28 in all PTMO-based materials. The number of repeat units (z) in the soft segment was about 39 for all PEO-based materials. The number (y) denotes the number of repeat units which is composed of HMDI and the chain extender for the PTMO-based samples. It is equal to 1.6 for high hard segment content sample in the first group and 0.6 for the low hard segment content one in the same group. For the second group, (y) is equal to 1.9 for the sample with HS = 30% and 0.7 for the sample with HS = 20%. Likewise, (w) is the number of repeat units for the PEO-based samples and is equal to 1.6 for the high hard segment content material in the third group and equal to 0.6 for the low hard segment content material in the same group. For the last group samples, (w) is equal to 1.9 for the sample with HS = 30% and to 0.7 for the sample with HS = 20%. The whole unit for the PTMO-based materials repeats n times, which is equal to 25 for PT-HMDA-30, 30 for PT-HMDA-20, 20 for PT-ED-30, and 25 for PT-ED-20. For the PEO-based materials the whole unit repeats m times, which is equal to 30 for PE-HMDA-30, 40 for PE-HMDA-20, 25 for PE-ED-30, and 30 for PE-ED-20.

Sample Preparation. Polymer films were prepared in Teflon molds by solvent casting. The solvent was first evaporated at room temperature overnight and then at 60 °C in an air oven and finally in a vacuum oven at 60 °C until constant weight was reached. The samples were kept in sealed polyethylene bags until testing. The cast films were cut into dumbbell shapes with narrowest width of 30 mm at 26 mm gauge length. The sample shape is designed so that it allows the use of transverse isotropy assumption safely.

Instrumentation. The stretching machine is designed to stretch both top and bottom cross-head in opposing directions in order to maintain midpoint observation point stationary. The spectral birefringence is measured from this midpoint using the automated system. The real time thickness was measured by using a laser micrometer mounted at an oblique angle that ensured the width measurement of the sample at the same position as the retardation measurement was made. The details of the instrumentation of real time measurement system can be found elsewhere.[19−21]

A Bruker AXS generator equipped with a copper target tube and a 2-D detector was used to obtain the unique quadrant of the uniaxially oriented samples. The generator was operated at 40 kV and 40 mA, and the beam was monochromatized at Cu Kα. An accumulation time of 20 min was used. The samples were placed 11.5 cm away from the detector.

Experimental Procedure. Two different loading procedures were applied on the samples: uniaxial stretching and hysteresis. For both procedures, the same specimen shape and dimensions whose details given above were used.

For the uniaxial stretching experiment, the specimen is mounted on the clamps and stretched up to an engineering stretch ratio of five that is the upper limit of the machine for these specimen dimensions. In the hysteresis experiments, the specimen was first stretched up to a engineering stretch ratio of 2 and then unloaded and loaded again to a higher stretch ratio with stretch ratio increments of 0.5. The reloading process is applied until the maximum possible stretching limit of the machine is reached. In all experiments, the samples were stretched at a rate of 25 mm/min.

The samples were captured at the stretched state by rectangular picture frame sandwich clamps. WAXS data were taken at a series of times extending to a few weeks while the specimen was maintained in the stretched state. This process was employed in order investigate the effects of stretching and long-term holding on crystallization. The portion of the material within the clamps is chosen carefully such that it includes

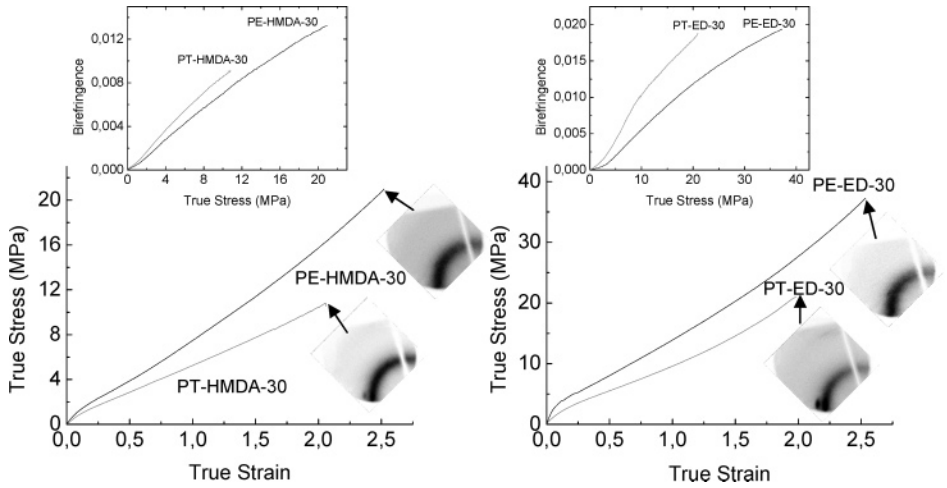

Figure 1. True stress vs true strain behavior of samples with different soft segments for HS = 30%.

the central point where the width and birefringence measurements are made. This allows birefringence data to be compared with X-ray data and observe the effect of crystallization on the birefringence−true stress curve.

Results and Discussion

Uniaxial Stretching and WAXS. The tensile behavior of thermoplastic elastomers generally depends on the (i) size, shape, and concentration of the hard domains,[22,23] (ii) intermolecular bonding within the hard domains, (iii) the ability of the soft segment to crystallize under strain,[10] and (iv) the extent of microphase separation. A high level of microphase separation in amine extended systems has been attributed to a larger number of possible H-bonds between hard segment chemical bonds.[15]

Effect of Soft Segment. Figure 1 shows the room temperature true stress−true strain−birefringence behavior of the materials whose hard segment concentration is 30 wt %. The curves are obtained from samples stretched to a stretch ratio of 5, which is smaller than the failure stretch ratios. To show the effect of soft segment, results for two samples with different soft segments but the same chain extender are compared on the same graph. WAXS data, shown in the figure, are taken at the state indicated by the arrows. The WAXS readings were taken offline while the specimen was being held in the stretched state by the clamps as explained above. The corresponding birefringence−true stress curves are given as insets in Figure 1.

As can be seen in Figure 1, interestingly, the samples based on PEO show larger true stress values than those with PTMO, regardless of the structure of the chain extender used. This may be due to the higher urea content of TPUUs based on amine-terminated PEO. On the other hand, since PTMO is hydroxy-terminated, it forms urethane groups during the prepolymer stage. Identical amounts of urea groups are generated during the chain extension in both systems. Since urea groups form much stronger intermolecular hydrogen bonding than urethanes,[24] PEO-based polymers show larger true stress values than those of their PTMO-based analogues. This observation is also supported by consideration of the differences in the glass transition temperature, T_g, values of −77 °C for PTMO and −55 °C for PEO. At room temperature, PEO is closer to its glass temperature and is therefore stiffer than PTMO. Difference in tensile strengths may also be due to higher

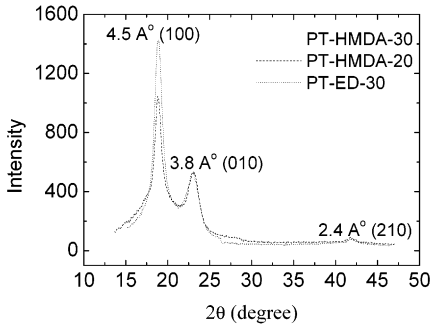

Figure 2. WAXS equatorial intensity profile for some PT samples stretched to a stretch ratio of 5.

cohesive energy density of PEO when compared with that of PTMO. This may result in slightly higher mixing between urea and ether and formation of a gradient interface between the hard and soft phases in PEO-based TPUUs. This in return may lead to a more efficient stress transfer from soft to hard phase and higher tensile strengths in PEO-based TPUUs.

When the crystallization patterns are investigated, it is seen that the unstretched sample whose soft segment is PTMO has an amorphous halo since the melting point of PTMO crystal (10 °C) is below room temperature at which the experiments are performed. After stretching, PTMO samples show crystallization upon deformation as indicated by the corresponding WAXS patterns in Figure 1. PTMO is known to be easily crystallizable, which explains this behavior. In a previous work, it was concluded by Yeh et al.[16] that the two peaks that can be observed starting from 200% strain are indicative of strain-induced crystallization of the PTMO. According to the same study, with the increase of strain (up to 700%), the crystalline regions become stronger and more oriented, whereas the unoriented amorphous phase becomes weaker. The equatorial intensity profiles from WAXS patterns at 500% strain are presented in Figure 2. It appears that PTMO-based samples show strain-induced crystallization with essentially needlelike crystals in which the polymer chains exhibit nearly perfect chain orientation with deformation. The WAXS pattern shown in Figure 2 indicates that the azimuthal distribution of equatorial crystalline peak is extremely narrow. This peak would not exist unless the polymer chains lose their entropy to create near perfect alignment. These results are in agreement with the conclusions of Bonart.[4]

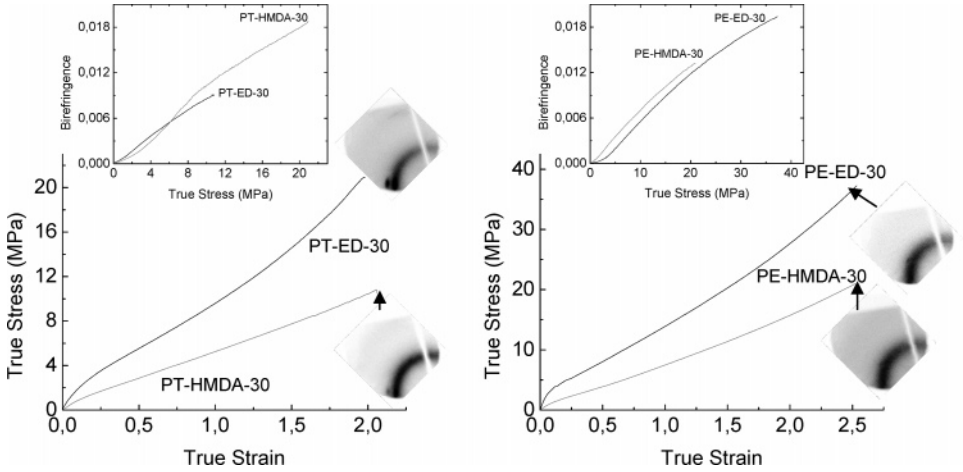

Figure 3. Effect of hard segment on true stress vs true strain for HS = 30%.

On the other hand, samples with PEO soft segments show little or no crystallization according to WAXS patterns taken right after the stretching, as can be seen from the X-ray patterns presented in Figure 1. This difference between the crystallization behaviors of the two soft segments can be explained as follows: The PT segment may be modeled as a chain of freely jointed rods where the butyl groups act as rods and the oxygen in between acts as the freely rotating joint. The PE segments are also similar, but the ethyl group constituting the stiff part is much shorter than the butyl group of PT. It is well-known that in chains of rigid rods separated by flexible joints crystallization takes place readily when the rodlike parts are longer.[25] Therefore, crystallization in PT samples is much more readily expected. The birefringence vs true stress curves of PT samples fall above the corresponding curves for the PEO segments.

Large Deformation Stress Optical Behavior. Collectively, the stress optical behavior of these materials can be categorized as "three-regime" behavior. Regime I, covering the lowest stress range, is the smallest of the three regimes. Following this regime, there is a rapid upturn into regime II that leads to regime III which has intermediate slope as the polymers presumably reach their finite extensibilities.

Inasmuch as birefringence is a measure of segmental orientation, these results indicate that the PTMO groups orient more than the PEO groups at corresponding strains.

Effect of Hard Segment. Figure 3 shows the room temperature true stress−true strain behavior of the materials whose hard segment concentration is 30%. The data are presented such that the samples that are based on the same soft segment are plotted on the same graph to show the effect of chain extender. The corresponding birefringence−true stress curves are given as insets in Figure 3. The samples with chain extender ED show larger true stress values than the ones with HMDA because each repeat unit of ED contains two CH_2 groups while that of HMDA contains six CH_2 groups, and the shorter chains are known to contribute more to stress at the same extension ratio. Irrespective of the soft segment type, the ED chain-extended ones exhibit higher crystallinity than the HMDA ones as can be seen from WAXS patterns in Figure 3. Wilkes et al.[8] observed two different types of order within the hard segment domains corresponding to two different chain extenders and attributed these to differences in the extent of molecular fit within the hard segments. This feature relates to entropy differences between the two types of chain extenders, ED $(CH_2)_2$ and HMDA $(CH_2)_6$. Assuming that each C−C bond can be in one of three possible rotational states, the number of different configurations which the two chain extenders can take may be estimated.[26,27] Since ED has a single rotatable bond, it can be in three different states in the network, whereas HMDA with five rotatable bonds can take up to 3^5 different configurations. This leads to larger entropy changes upon deformation of HMDA extended ones than ED. As a result of this difference, samples with the ED have little entropy to lose upon stretching and readily crystallize, whereas the ones containing HMDA has a large amount of entropy to lose and is therefore more difficult to crystallize. It is also worth noting that HMDA acts like a more flexible hinge for the two rigid segments flanking it on its both sides. Alternatively, ED acts like a stiffer hinge for its flanking rigid neighbors.

Effect of Hard Segment Concentration (HS = 20% vs HS = 30%). Although the samples with hard segment content of 30% have been used to explain the effect of soft and hard segments in the discussion above, a comparison with the ones with HS = 20% can be helpful in explaining the contribution of hard segment concentration to mechanical behavior.

Figure 4 gives the true stress−true strain−birefringence data for PT−HMDA samples whose hard segment percentages is either 20% or 30%. The left panel shows the stress−strain results, and the right panel shows the birefringence results. As can be seen from this figure, the PT sample with higher hard segment concentration shows larger true stress values. This is expected since the hard segment is the part which gives high strength characteristics to TPUUs. When compared from crystallization point of view, a better orientation scheme is observed in the low hard segment content sample. Upon decreasing the hard segment content, a transition of morphology from interconnecting hard and soft segment domains to isolated hard segment domains in a soft segment matrix was observed by Cooper et al.[10] This may explain the better phase separation and crystal structure in PT samples with the low hard segment content.

Figure 5 shows the true stress−strain values for PT−ED samples with HS = 20% and HS = 30%. Again, the sample with higher hard segment concentration shows larger true stress values. The third peak that is observed at about $2\theta = 42.5°$ in Figure 2 is slightly

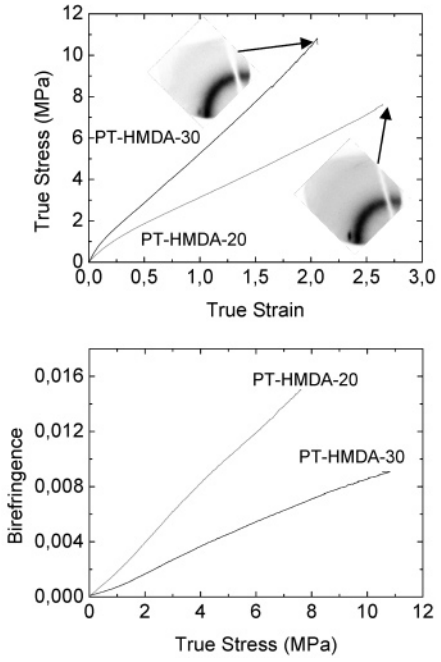

Figure 4. True stress−true strain−birefringence values for PT-HMDA with HS = 20% and HS = 30%.

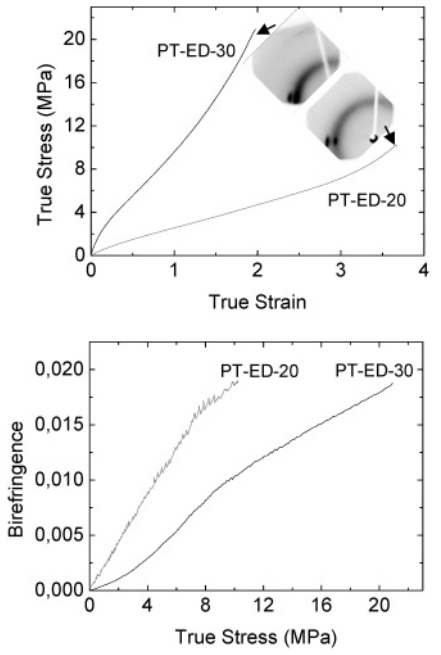

Figure 5. True stress−true strain−birefringence values for PT-ED with HS = 20% and HS = 30%.

observable in the upper left portion of the WAXS pattern of 30% sample but cannot be seen for 20%. This peak was attributed to strain-induced crystallization of PT.[16] So it can be said that strain-induced crystallization of PT is more pronounced as hard segment content increases.

In Figure 6, true stress−true strain−birefringence data for PE-HMDA-20 and PE-HMDA-30 are given. The same behavior, namely, larger stress values for high hard segment concentration, can be observed for PE-HMDA. However, there is no crystallization for both PE-HMDA samples, which may clearly be attributed to the role of the PE groups, as discussed above.

True stress−true strain−birefringence graphs for PE-ED samples with different hard segment contents

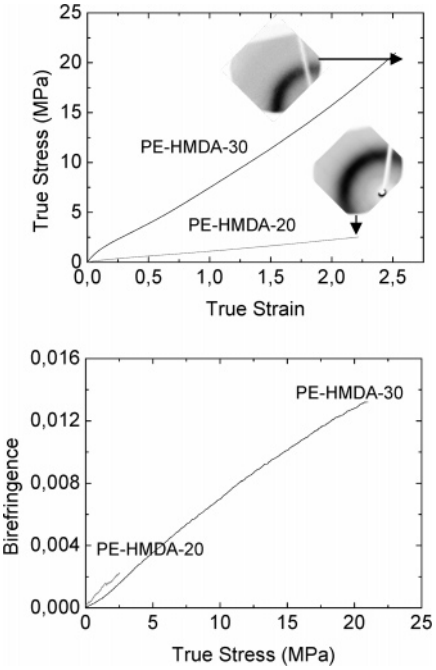

Figure 6. True stress−true strain−birefringence values for PE-HMDA with HS = 20% and HS = 30%.

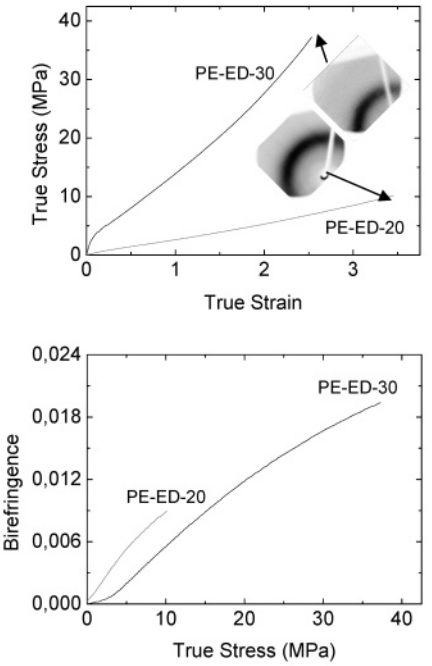

Figure 7. True stress−true strain−birefringence values for PE-ED with HS = 20% and HS = 30%.

(either HS = 20% or HS = 30%) are plotted in Figure 7. There is a remarkable effect of hard segment concentration on the stress−optical behavior. Regime I present in the PE-ED-30 is suppressed in PE-ED-20 where only the linear stress optical rule followed by saturation at high stresses is observed. Both samples undergo crystallization and exhibit near perfect chain orientation along the stretching direction as may be seen from the WAXS data. While PE-ED-20 containing smaller fraction of hard segments forms a well-organized three-dimensional lattice structure (presence of off-equatorial peaks and their sharpness indicates this), increasing hard segment content appear to suppress this organization as the crystalline peaks are slightly broader.

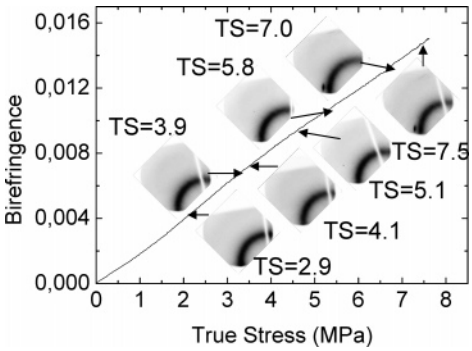

Figure 8. WAXS data taken at different true stress values for PT-HMDA-20.

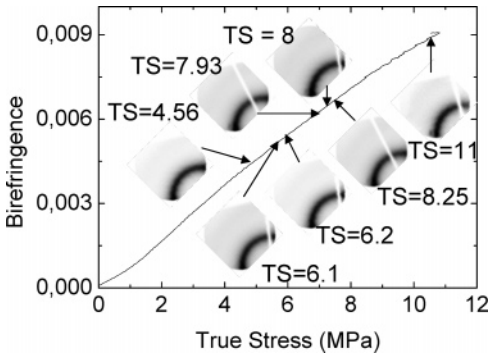

Figure 9. WAXS data taken at different true stress values for PT-HMDA-30.

This is most likely due to steric hindrance effect on crystallizing species in the presence of larger fraction of rigid hard segments.

X-ray data at different stretch ratios of PT-HMDA for HS = 20% and HS = 30% can be seen in Figure 8 and Figure 9, respectively. The true stress values at which the WAXS readings are made are indicated by TS in the figures.

When Figure 8 is compared with Figure 9, it is quite interesting to observe that the crystallization sets in at very high true strain values for the low hard segment concentration sample but spreads out more on the PT-HMDA-30. The crystallization is accompanied by a slight upturn on birefringence−true stress curve in PT-HMDA-20. It is important to note that at least three stress optical regimes are discernible in both Figures 8 and 9. The initial linear regime gives way to regime II with steeper slope near 1−2 MPa. This slightly longer regime straightens out at higher stress levels. Remarkably, we do not see any evidence of expected leveling off in these curves. In fact, we note a slight further positive deviation accompanying the appearance of equatorial diffraction peaks. In the absence of off-equatorial peaks this peak can be categorized as "nematic-like" as it exhibits the above-mentioned near perfect orientation (Figure 8). The evolution of the crystalline peak is more gradual in PT-HMDA-30. But the developed equatorial peak is broader, indicating lateral packing order of these "nematic-like" regions is poorer, presumably reflecting the steric hindrance effects of the increased population of hard segments.

The true stress−true strain curves of the same materials (PT-HMDA-20 on the left and PT-HMDA-30 on the right) at different strain rates and corresponding WAXS patterns are presented in Figure 10. The rates 2, 25, and 200 mm/min are indicated in the figure. For both materials, the largest stress values are observed for the fastest strain rate. The low hard segment content PT sample shows better crystallization when stretched at the slowest rate, 2 mm/min. Crystallization decreases with increasing strain rate as can be seen from the respective WAXS data in Figure 10. On the other hand, the crystallization of high hard segment content PT is the opposite, and crystallization increases with increasing strain rate.

There is considerable detail in the WAXS patterns of PT-HMDA-20 and PT-HMDA-30 as they are affected by the stretching rate. The PT-HMDA-20 sample containing smaller fraction of hard segment exhibits lower orientation (compare the azimuthal spread of the equatorial nematic-like diffraction peak) as compared to those of PT-HMDA-30. In addition, the faster the stretching rate is employed the narrower this peak becomes in PT-HMDA-20. This suggests that at slower deformation rates more of the crystallizable segments—however disorganized they are—get into registry with one another and contribute to this peak if they are sufficiently oriented parallel to one another. Increasing stretching rate (suppression of relaxation mechanism) eliminate the formation of the latter disordered regions that are responsible for broadening the equatorial peak at low rates. Clearly, PT-HMDA-30 data indicate that the crystallizable segments need to be more oriented to register with one another (lower azimuthal spread) to contribute to the broader equatorial peak; otherwise, they would not exist at all. Faster stretching certainly promotes this mechanism in the presence of higher fraction of hard segments.

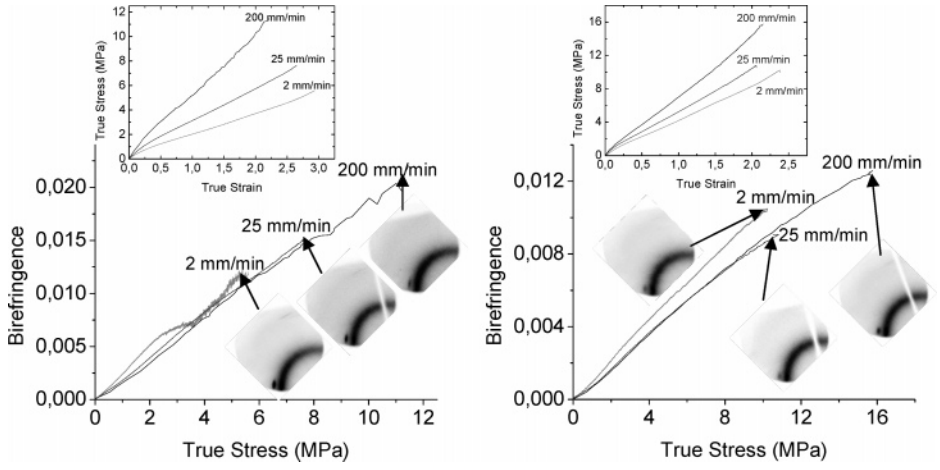

Figure 10. True stress−true strain curves for PT-HMDA-20 and PT-HMDA-30 at different strain rates.

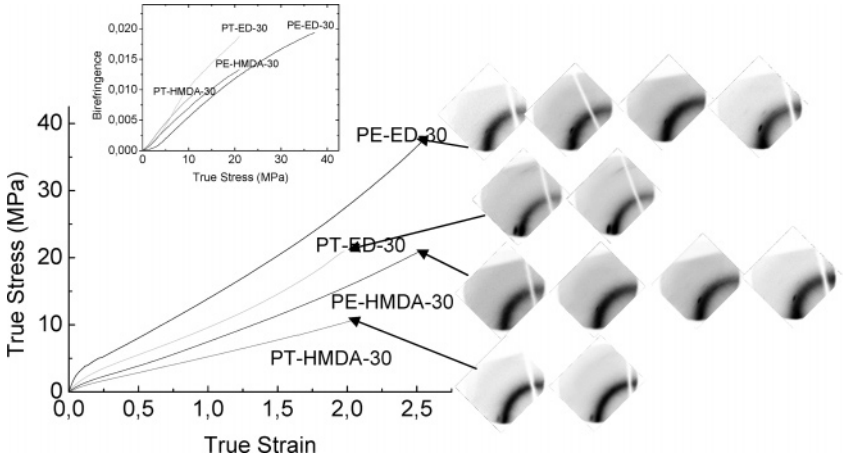

Figure 11. True stress vs true strain for HS = 30% (general behavior).

General Behavior for HS = 30%. In Figure 11, we compare the true stress−true strain and birefringence−true stress behavior of all HS = 30% samples. The measurements are coupled with repeated offline WAXS data taken at the strains indicated by the arrows. The first WAXS is taken right after the stretching, and the rest is taken in the following days (1 day between each experiment) while the specimen is still kept at the stretched position within the clamps. The effects of soft and hard segments of the same samples were explained earlier. All materials display the typical behavior of elastomers, with stress−strain behavior primarily depending on composition. It was also observed from the experiments that have been carried on a standard Instron machine that PE series extend to much higher stretch ratios than PT. Since elongation is usually related to soft segments, this can be attributed to the characteristic behavior of PEO that gives the material more flexibility than PTMO. The interesting point in the WAXS patterns is the crystallization behavior of the PE samples. As explained above, PE samples show little (PE-ED-30) or no crystallization (PE-HMDA-30) at the end of stretching. But while the sample is kept at the stretched position within the clamp, the PE-ED-30 sample gradually developed highly oriented crystalline peaks superposed to amorphous halo over time. During this holding stage the relaxation gradually brings the chains that were highly oriented but unregistered to laterally and axially registered state for them to form three-dimensionally ordered crystalline state. This is quite pronounced in PE-ED-30 and PE-HMDA-30.

Figure 11 also shows the birefringence vs true stress values for the samples with HS = 30%. The stress optical law relates the birefringence and stresses applied in a system. The law follows a linear behavior of the birefringence with the stress as shown by the equation $\Delta n = C\sigma$, where Δn is the birefringence, C is the stress optical constant, and σ is the stress.

An increase in birefringence is observed beginning from the start of stretching. Real-time birefringence system data allow us to observe a very small linear portion on the true stress vs birefringence curves, which obeys the stress optical law. The reason for this is because these materials should not be considered similar to standard amorphous materials. The main reason is because the hard segments are forming the long-range physical network and since they exist at very early stages, and then they rapidly make this relationship nonlinear. According to past experience,[28] prior to crystallization linearity of birefringence stress is preserved. But if crystallization is induced, nonlinearity is acquired immediately due to long-range connectivity through the connected formed crystallites together with entanglements and hydrogen bonds. The stress optical coefficients for all samples may be determined from the linear portion of the birefringence vs true stress curves (Figure 11) and by the use of stress−optical law. The results are presented in Table 3.

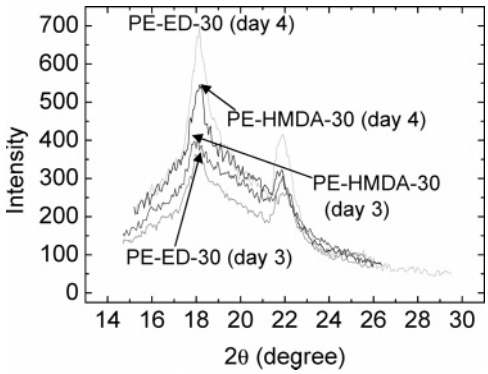

Figure 12. WAXS equatorial intensity profile for some PE samples stretched to 500%.

Table 3. Stress Optical Constants in GPa^{-1} from Stretching Data

PT-HMDA-20	1.8	PT-HMDA-30	0.3
PT-ED-20	2.2	PT-ED-30	0.4
PE-HMDA-20	1.0	PE-HMDA-30	0.4
PE-ED-20	0.9	PE-ED-30	0.1

Hysteresis and WAXS. The mechanical hysteresis of a polymer represents the fractional energy lost as a result of subjecting that material to a defined deformation cycle. As with other elastomers, it can occur in polyurethanes due to a number of mechanisms such as (i) internal friction as segments of polymer molecules slide past each other as the molecules change their conformations during the deformation cycle, (ii) formation and rupture of hydrogen bonds under deformation, and (iii) strain-induced crystallization as aligned segments crystallize during loading and plastic deformation of the second phase domains.[29]

The true stress−strain hysteresis curves for the materials stretched to 2×, 2.5×, 3×, and 3.5× at room temperature and subsequently retracted to zero strain are presented in Figure 13. WAXS data are taken at the end of 4× while the specimen was being held within the clamps as explained above. The first WAXS pattern

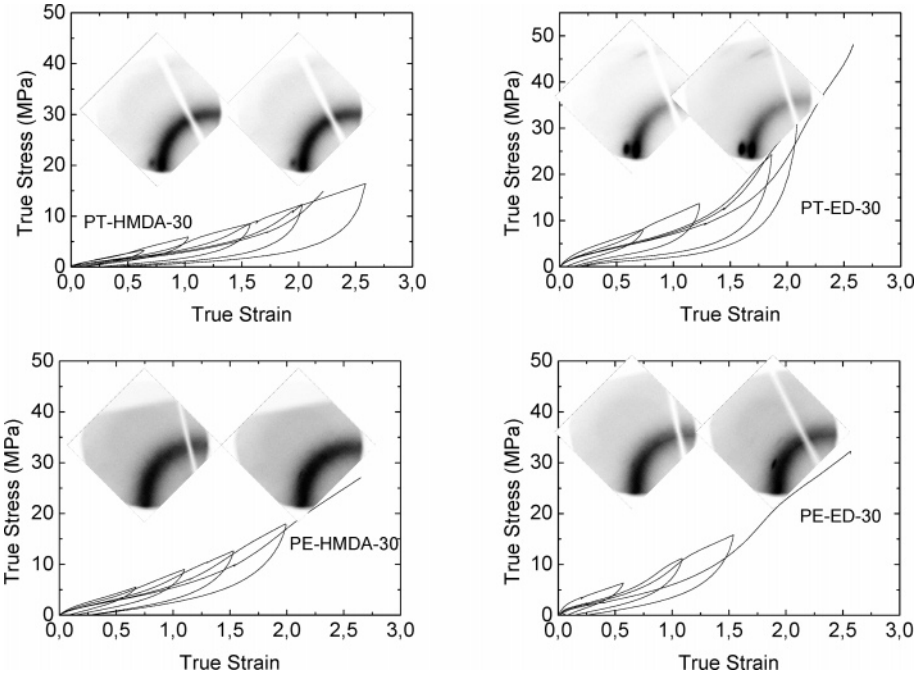

Figure 13. Hysteresis true stress−true strain values for HS = 30%.

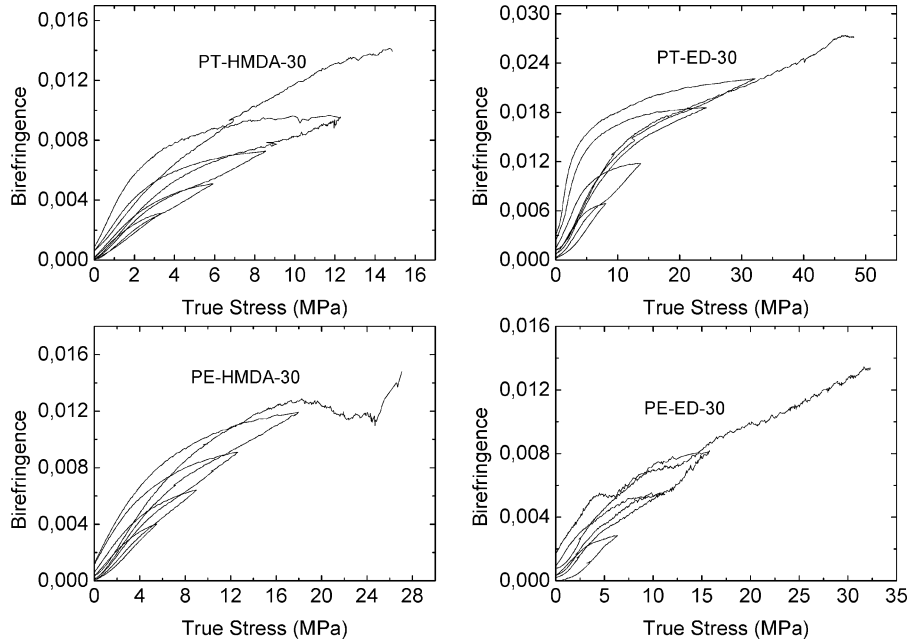

Figure 14. Hysteresis birefringence values for HS = 30%.

was taken right after the stretching, and the second one was taken 1 day later while the specimens were held stretched within the frames. The corresponding birefringence graphs are plotted in Figure 14.

For all the samples, the hysteresis loop (thus the energy lost) increases as the stretch ratio in cyclic loading increases. The greatest increase is observed for PT-ED (most crystalline sample) and the smallest for PE-HMDA (least crystalline sample). This is due to different mechanisms of deformation operating during stretching and retracting. During stretching, the molecules are reorganized, aligning themselves along the stretching direction. If the deformation is high enough, some of the chemical bonds, specifically the hydrogen bonds, can break, leading to disentanglement in the network. Rupturing of the hydrogen bonds leads to molecular slippage, chain disentanglement, phase mixing, soft segment crystallization, and the re-formation of new bonds in the stretch configuration.[18] As deformation increases, crystalline regions begin to form, making the network more complex. On retraction from high deformations, the network cannot recover totally. This leads to an energy difference that can be observed as a loop at the stress−strain curve. This kind of energy loss is less pronounced for lower stretch ratios where permanent deformation hardly takes place.

The only difference between the crystallization patterns of the samples subject to hysteresis and the ones stretched uniformly is that the crystals are more clearly observable under hysteresis, showing that cyclic loading−unloading of the samples finally results in better orientation of the polymer network than simply stretching. The unique crystallization behavior of PE samples (crystallization under relaxation) is again observed in

hysteresis. There is also considerable hysteresis and a very small linear region in birefringence graphs.

Conclusions

Eight different samples were synthesized by selectively varying the amount and type of soft and hard segments. The effect of these changes on the mechano-optical properties was examined by uniaxial stretching and hysteresis experiments coupled with offline WAXS.

All of the PTMO-based samples showed the two crystalline diffraction peaks at the same 2θ angle which is characteristic of PTMO. On the other hand, PEO-based samples showed little or no crystallization at the end of stretching. The polymers with ED chain extender showed higher crystallizability no matter which soft segment was used.

While the increase of hard segment content resulted in larger true stress values, their reduction lead to improved strain crystallizabilities regardless of the material composition. Strain-induced crystallization of PTMO becomes more pronounced as the hard segment content in the sample increases. The strain rate has a considerable effect on the crystallization behavior of two PTMO-based materials. While crystallization in PT-HMDA-20 decreases with increasing strain rate, it increases for the PT-HMDA-30 sample. Although the PEO-based sample showed little or no crystallization right after stretching, it was found to develop oriented crystalline structure over time while the stretched sample is kept in the constrained state.

The birefringence−true stress curves had very small linear regions for all materials. This was attributed to presence of phase-segregated structures in these materials that act as long-range physical network, causing the deviation from the initial linear stress optical behavior. Hysteresis was observed in all samples. As the stretch ratio increased, the amount of hysteresis also increased. When the WAXS patterns are compared for all samples, we observe better crystalline order in samples that has undergone multiple cycles of stretching during hysteresis as compared to those stretched once. This may be attributed to the reduction of steric hindrance on the crystallizable segments by loosening the physical network, a process that may involve breakage of inter- and intrachain hydrogen bonding.

Acknowledgment. The authors gratefully acknowledge the International travel grant provided by NSF-US-Turkey travel Grant #INT-9974598.

References and Notes

(1) Cooper, S. L.; Tobolsky, A. V. *J. Appl. Polym. Sci.* **1966**, *10*, 1837−1844.
(2) Clough, S. B.; Schneider, N. S. *J. Macromol. Sci., Phys.* **1968**, *B2*, 553−566.
(3) Clough, S. B.; Schneider, N. S.; King, A. O. *J. Macromol. Sci., Phys.* **1968**, *B2*, 641−648.
(4) Bonart, R. *J. Macromol. Sci., Phys.* **1968**, *B2*, 115−138.
(5) Chang, Y. J. P.; Wilkes, G. L. *J. Polym. Sci., Phys.* **1975**, *13*, 455−476.
(6) Estes, G. M.; Seymour, R. W.; Cooper, S. L. *Macromolecules* **1971**, *4*, 452−457.
(7) Bonart, R.; Mobitzer, L.; Muller, E. D. *J. Macromol. Sci., Phys.* **1974**, *B9*, 447−461.
(8) Wilkes, C. E.; Yusek, C. S. *J. Macromol. Sci., Phys.* **1973**, *B7*, 157−175.
(9) Sung, C. S. P.; Sung, N. H.; Smith, T. W. *Macromolecules* **1980**, *13*, 117−121.
(10) Cooper, S. L.; Wang, C. B. *Macromolecules* **1983**, *16*, 775−786.
(11) Fu, B.; Macknight, W. J.; Schneider, N. S. *Rubber Chem. Technol.* **1986**, *59*, 896−911.
(12) Meuse, C. W.; Yang, X.; Yang, D.; Hsu, S. L. *Macromolecules* **1992**, *25*, 925−926.
(13) Koberstein, J. T.; Galambos, A. F.; Leung, L. M. *Macromolecules* **1992**, *25*, 6195−6204.
(14) Cooper, S. L.; Hwang, K. S.; Lin, S. B.; Tsay, S. Y. *Colloid Polym. Sci.* **1985**, *263*, 128−140.
(15) Desper, C. R.; Jasinski, J. P.; Lin, J. S.; Schneider, N. S. *Macromolecules* **1985**, *18*, 2755−2761.
(16) Yeh, F.; Hsiao, B. S.; Sauer, B. B.; Michel, S.; Siesler, H. W. *Macromolecules* **2003**, *36*, 1940−1954.
(17) Allegrezza, A. E.; Cooper, S. L.; Seymour, R. W. *Macromolecules* **1973**, *6*, 896−902.
(18) Gorce, J. N.; Hellgeth, J. W.; Ward, T. C. *Polym. Eng. Sci.* **1993**, *33*, 1170−1176.
(19) Toki, S.; Valladares, D.; Sen, T. Z.; Cakmak, M. *SPE ANTEC Technol. Pap.* **2001**, 1830−1834.
(20) Valladares, D.; Toki, S.; Sen, T. Z.; Yalcin, B.; Cakmak, M. *Macromol. Symp.* **2002**, *185*, 149−166.
(21) Koike, Y.; Cakmak, M. *Polymer* **2003**, *44*, 4249−4260.
(22) Nielsen, L. E. *Rheol. Acta* **1974**, *13*, 594−600.
(23) Aggarwal, S. L. *Block Polymers*; Plenum Press: New York, 1970.
(24) Yilgor, E.; Yilgor, I.; Yurtsever, E. *Polymer* **2002**, *43*, 6551−6559.
(25) Bahar, I.; Erman, B.; Kloczkowski, A.; Mark, J. E. *Macromolecules* **1990**, *23*, 5335−5341.
(26) Flory, P. J. *Statistical Mechanics of Chain Molecules*; Wiley-Interscience: New York, 1969 (reprinted by Hanser, Munchen, 1989).
(27) Mattice, W. L.; Suter, U. W. *Conformational Theory of Large Molecules. The Rotational Isomeric State Model in Macromolecular Systems*; John Wiley & Sons: New York, 1994.
(28) Mulligan, J. H.; Cakmak, M. *Annu. Tech. Conf.—Soc. Plast. Eng.* **2003**, *61st* (Vol. 2), 1588−1592.
(29) Beck, R. A.; Truss, R. W. *J. Appl. Polym. Sci.* **1999**, *71*, 959−966.
(30) Bonart, R.; Müller-Riederer, G. *Colloid Polym. Sci.* **1981**, *259*, 926−936.

MA049018A